The number of adventitial lymphatic vessels was reduced in the GSV, suggesting that dysfunction of lymph transport and subsequent lymph congestion might occur. Because lymphatic fluid contains high concentrations of lipid molecules, such as PC and TG, lymphatic stasis causes tissue accumulation of lipid molecules.[26,29] Taken together, the abnormal accumulation of various lipid molecules may be associated with disturbances in lymph transport due to the loss of lymph vessels. The association of lymphatic dysfunction with VVs remains to be determined.

Because venodynamics and lymphodynamics interact as an inseparable and mutually dependent dual outflow system in tissue, the system is complex. Homeostasis can only be maintained by a balance between the two systems. The degeneration of VV tissue may be associated with increased permeability, which could cause elevation of tissue pressure and perivascular inflammation. The elevation of tissue pressure induces not only lymphatic vessel dysfunction but also structural damages to the microlymphatic networks.[30]

The resultant lymph stasis is associated with chronic inflammation.[31] Moreover, the inflammation due to cytokines, such as tumor necrosis factor-α, may induce apoptosis of the lymphatic vessel and decrease the number of the vessels.[32] These mixed venous and lymphatic disorders are known as phlebolymphedema.[33,34] In fact, patients with chronic venous insufficiency have microangiopathy of the lymphatic network.[35] We used indocyanine green fluorescence lymphography in a previous study to show that the speed of lymph transportation in the lower leg was reduced in VV patients, suggesting that secondary phlebolymphedema could occur in chronic venous insufficiency.[36] A study that used dynamic lymphoscintigraphy in VV patients reported a similar finding.[37]

The abnormal distribution of lipid molecules in VV tissue observed in both VV groups suggests that VV-associated accumulation of lipid molecules begins in the early clinical stages of the disease and continues through the advanced stages. In particular, the accumulation of LPC (1-acyl 16:0) and PC (diacyl 16:0/20:4) in the media was significantly higher in VV tissue from patients in advanced clinical stages, suggesting an association between lipid accumulation and chronic inflammation of the skin and subcutaneous tissues.

One limitation of this study was that the control veins came from peripheral arterial disease patients, and these veins might have been metabolically affected by the disease. Moreover, GSV from patients with VV might have various histochemical changes, depending on the segments,[38] which would require the harvest of multiple segments of the GSV samples for assessment of the distribution of the lipid molecules.

Further study is needed to clarify the effect of lymph stasis on VVs and chronic inflammation. The mechanism whereby adventitial lymphatic vessels are damaged is also unknown. Consistent venous hypertension and subsequent overload to the lymphatics may account for the lymphatic damage.[30] In addition, accumulation of possible proinflammatory lipid molecules in VV walls may further damage the adventitial lymphatic vessels.

CONCLUSIONS

The accumulation of LPC (1-acyl 16:0) and PC (diacyl 16:0/20:4) in VV tissue may be associated with chronic inflammation, leading to VV tissue degeneration. Moreover, the number of lymphatic vessels in the adventitia of VV tissue is significantly less than that of control tissue. Loss of lymphatic vessels may be associated with the accumulation of lipid molecules and subsequent degeneration of the vein wall in VVs.

We are grateful to Tsuyako Ida, Kinue Hatano, and Yumi Kaneko for their technical assistance.

AUTHOR CONTRIBUTIONS

Conception and design: NU
Analysis and interpretation: HT, NZ, TS, MS
Data collection: HT, NY, NS
Writing the article: HT, NU
Critical revision of the article: HK, MS, NU
Final approval of the article: NU
Statistical analysis: HT
Obtained funding: NU
Overall responsibility: NU

REFERENCES

1. Tanaka H, Zaima N, Yamamoto N, Sagara D, Suzuki M, Nishiyama M, et al. Imaging mass spectrometry reveals unique lipid distribution in primary varicose veins. Eur J Vasc Endovasc Surg 2010;40:657-63.
2. Henriksen JR, Andresen TL, Feldborg LN, Duelund L, Ipsen JH. Understanding detergent effects on lipid membranes: a model study of lysolipids. Biophys J 2010;98:2199-205.
3. Koizumi S, Yamamoto S, Hayasaka T, Konishi Y, Yamaguchi-Okada M, Goto-Inoue N, et al. Imaging mass spectrometry revealed the production of lyso-phosphatidylcholine in the injured ischemic rat brain. Neuroscience 2010;168:219-25.
4. Yang HJ, Ishizaki I, Sanada N, Zaima N, Sugiura Y, Yao I, et al. Detection of characteristic distributions of phospholipid head groups and fatty acids on neurite surface by time-of-flight secondary ion mass spectrometry. Med Mol Morphol 2010;43:158-64.
5. Lim CS, Davies AH. Pathogenesis of primary varicose veins. Br J Surg 2009;96:1231-42.
6. Bergan JJ, Pascarella L, Schmid-Schönbein GW. Pathogenesis of primary chronic venous disease: insights from animal models of venous hypertension. J Vasc Surg 2008;47:183-92.
7. Eklöf B, Rutherford RB, Bergan JJ, Carpentier PH, Gloviczki P, Kistner RL, et al. Revision of the CEAP classification for chronic venous disorders: consensus statement. J Vasc Surg 2004;40:1248-52.
8. Yamamoto N, Unno N, Mitsuoka H, Saito T, Miki K, Ishimaru K, et al. Preoperative and intraoperative evaluation of diameter-reflux relationship of calf perforating veins in patients with primary varicose vein. J Vasc Surg 2002;36:1225-30.
9. Shrivas K, Hayasaka T, Goto-Inoue N, Sugiura Y, Zaima N, Setou M. Ionic matrix for enhanced MALDI imaging mass spectrometry for identification of phospholipids in mouse liver and cerebellum tissue sections. Anal Chem 2010;82:8800-6.
10. Morita Y, Ikegami K, Goto-Inoue N, Hayasaka T, Zaima N, Tanaka H, et al. Imaging mass spectrometry of gastric carcinoma in formalin-fixed paraffin-embedded tissue microarray. Cancer Sci 2010;101:267-73.
11. Hayasaka T, Goto-Inoue N, Zaima N, Kimura Y, Setou M. Organ-specific distributions of lysophosphatidylcholine and triacylglycerol in mouse embryo. Lipids 2009;44:837-48.

12. Sugiura Y, Konishi Y, Zaima N, Kajihara S, Nakanishi H, Taguchi R, et al. Visualization of the cell-selective distribution of PUFA-containing phosphatidylcholines in mouse brain by imaging mass spectrometry. J Lipid Res 2009;50:1776-88.
13. Zaima N, Sugawara T, Goto D, Hirata T. Trans geometric isomers of EPA decrease LXRalpha-induced cellular triacylglycerol via suppression of SREBP-1c and PGC-1beta. J Lipid Res 2006;47:2712-7.
14. Elsharawy MA, Naim MM, Abdelmaguid EM, Al-Mulhim AA. Role of saphenous vein wall in the pathogenesis of primary varicose veins. Interact Cardiovasc Thorac Surg 2007;6:219-24.
15. Wali MA, Eid RA. Smooth muscle changes in varicose veins: an ultrastructural study. J Smooth Muscle Res 2001;37:123-35.
16. Xiao Y, Huang Z, Yin H, Lin Y, Wang S. In vitro differences between smooth muscle cells derived from varicose veins and normal veins. J Vasc Surg 2009;50:1149-54.
17. Travers JP, Brookes CE, Evans J, Baker DM, Kent C, Makin GS, et al. Assessment of wall structure and composition of varicose veins with reference to collagen, elastin and smooth muscle content. Eur J Vasc Endovasc Surg 1996;11:230-7.
18. Meissner MH, Gloviczki P, Bergan J, Kistner RL, Morrison N, Pannier F, et al. Primary chronic venous disorders. J Vasc Surg 2007;46(Suppl S):54-67S.
19. Rizzi A, Quaglio D, Vasquez G, Mascoli F, Amadesi S, Calò G, et al. Effects of vasoactive agents in healthy and diseased human saphenous veins. J Vasc Surg 1998;28:855-61.
20. Wali MA, Eid RA. Changes of elastic and collagen fibers in varicose veins. Int Angiol 2002;21:337-43.
21. Zaima N, Sasaki T, Tanaka H, Cheng XW, Onoue K, Hayasaka T, et al. Imaging mass spectrometry-based histopathologic examination of atherosclerotic lesions. Atherosclerosis 2011;217:427-32.
22. Pascarella L, Schmid-Schönbein GW, Bergan J. An animal model of venous hypertension: the role of inflammation in venous valve failure. J Vasc Surg 2005;41:303-11.
23. Kume N, Gimbrone MA, Jr. Lysophosphatidylcholine transcriptionally induces growth factor gene expression in cultured human endothelial cells. J Clin Invest 1994;93:907-11.
24. Lim CS, Gohel MS, Shepherd AC, Palcolog E, Davies AH. Venous hypoxia: a poorly studied etiological factor of varicose veins. J Vasc Res 2011;48:185-94.
25. Takase S, Pascarella L, Bergan JJ, Schmid-Schönbein GW. Hypertension-induced venous valve remodeling. J Vasc Surg 2004;39:1329-34.
26. Nanjee MN, Cooke CJ, Olszewski WL, Miller NE. Lipid and apolipoprotein concentrations in prenodal leg lymph of fasted humans. Associations with plasma concentrations in normal subjects, lipoprotein lipase deficiency, and LCAT deficiency. J Lipid Res 2000;41:1317-27.
27. Liu E, Goldhaber JI, Weiss JN. Effects of lysophosphatidylcholine on electrophysiological properties and excitation-contraction coupling in isolated guinea pig ventricular myocytes. J Clin Invest 1991;88:1819-32.
28. Balsinde J, Dennis EA. Function and inhibition of intracellular calcium-independent phospholipase a2. J Biol Chem 1997;272:16069-72.
29. Bennuru S, Maldarelli G, Kumaraswami V, Klion AD, Nutman TB. Elevated levels of plasma angiogenic factors are associated with human lymphatic filarial infections. Am J Trop Med Hyg 2010;83:884-90.
30. Zawieja DC. Contractile physiology of lymphatics. Lymph Res Biol 2009;7:87-96.
31. Tabibiazar R, Cheung L, Han J, Swanson J, Beilhack A, An A, et al. Inflammatory manifestations of experimental lymphatic insufficiency. PLoS Med 2006;3:e254.
32. Niemann-Jönsson A, Ares MP, Yan ZQ, Bu DX, Fredrikson GN, Brånén L, et al. Increased rate of apoptosis in intimal arterial smooth muscle cells through endogenous activation of TNF receptors. Arterioscler Thromb Vasc Biol 2001;21:1909-14.
33. Bunke N, Brown K, Bergan BJ. Phlebolymphemeda: usually unrecognized, often poorly treated. Perspect Vasc Surg Endovasc Ther 2009;21:65-8.
34. Piller N. Phlebolymphoedema/chronic lymphatic insufficiency: an introduction to strategies for detection, differentiation and treatment. Phlebology 2009;24:51-5.
35. Franzeck UK, Haselbach P, Speiser D, Bollinger A. Microangiopathy of cutaneous blood and lymphatic capillaries in chronic venous insufficiency (CVI) Yale. J Biol Med 1993;66:37-46.
36. Suzuki M, Unno N, Yamamoto N, Nishiyama M, Sagara D, Tanaka H, et al. Impaired lymphatic function recovered after great saphenous vein stripping in patients with varicose vein: venodynamic and lymphodynamic results. J Vasc Surg 2009;50:1085-91.
37. Mortimer PS. Evaluation of lymphatic function: Abnormal lymph drainage in venous disease. Int Angiol 1995;14:32-5.
38. Badier-Commander C, Couvelard A, Henin D, Verbeuren T, Michel JB, Jacob MP. Smooth muscle cell modulation and cytokine overproduction in varicose veins. An in situ study J Pathol 2001;193:398-407.

Submitted Aug 7, 2011; accepted Sep 17, 2011.

analytical chemistry

ARTICLE

pubs.acs.org/ac

Method for Simultaneous Imaging of Endogenous Low Molecular Weight Metabolites in Mouse Brain Using TiO_2 Nanoparticles in Nanoparticle-Assisted Laser Desorption/Ionization-Imaging Mass Spectrometry

Kamlesh Shrivas, Takahiro Hayasaka, Yuki Sugiura, and Mitsutoshi Setou*

Department of Cell Biology and Anatomy, Hamamatsu University School of Medicine, 1-20-1 Handayama, Higashi-ku, Hamamatsu, Shizuoka 431-3192, Japan

Supporting Information

ABSTRACT: We report the detection of a group of endogenous low molecular weight metabolites (LMWM) in mouse brain (80−500 Da) using TiO_2 nanoparticles (NPs) in nanoparticle-assisted laser desorption/ionization-imaging mass spectrometry (Nano-PALDI-IMS) without any washing and separation step prior to MS analysis. The identification of metabolites using TiO_2 NPs was compared with a conventional organic matrix 2,5-dihydroxybenzoic acid (DHB) where signals of 179 molecules were specific to TiO_2 NPs, 4 were specific to DHB, and 21 were common to both TiO_2 NPs and DHB. The use of TiO_2 NPs enabled the detection of a higher number of LMWM as compared to DHB and gold NPs as a matrix. This approach is a simple, inexpensive, washing, and separation free for imaging and identification of LMWM in mouse brain. We believe that the biochemical information from distinct regions of the brain using a Nano-PALDI-IMS will be helpful in elucidating the imbalances linked with diseases in biomedical samples.

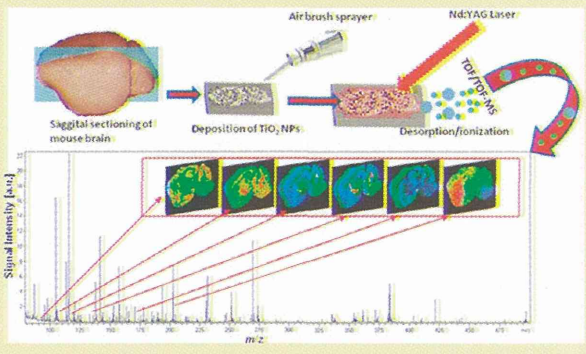

The brain is the central part of the nervous system, and it monitors and regulates the body's actions and reactions. The presence of endogenous low molecular weight metabolites (LMWM) in brain has important role in biosynthesis, product degradation, energy production, signaling, and defense.[1] Recent advances in molecular imaging modalities have opened opportunities for molecular diagnostic and therapeutic procedures. Magnetic resonance imaging (MRI) and positron emission tomography (PET) are known noninvasive techniques in imaging for medical diagnosis and also used for obtaining biochemical information from living tissue in order to establish the presence of any disorder.[2,3] Nuclear magnetic resonance spectroscopy (NMRS) imaging is also helpful for the identification of LMWM in brain. So far, with NMRS imaging, only a few molecules are reported which are highly abundant in the brain.[4] The limitations of these techniques are relatively poor resolution, sensitivity, and requirement of labeling of molecules for the detection (in the case of PET method). Liquid chromatography−mass spectrometry (LC-MS) is normally used for the analysis of LMWM in tissue samples.[5] Petyuk et al. demonstrated the mapping of abundance protein in brain using voxelation in combination with LC-MS. This approach provided a procedure to image the brain proteome in the adult and also to understand the etiology of neurodegenerative and other brain disorders.[6] However, this technique requires tedious sample preparation and longer analysis time.

Nowadays, matrix-assisted laser desorption/ionization mass spectrometry (MALDI-MS) is proven to be a simple and rapid tool available to researchers in biochemistry and molecular biology for the identification of biomolecules.[7] However, the analysis of LMWM (<500 Da) is limited in MALDI-MS applications because of the organic matrix-oriented low mass interferences. Therefore, inorganic and nanomaterials are introduced as the matrix in order to reduce the drawbacks of organic matrixes in the MALDI-MS analysis. Tanaka et al. first reported the application of a 30 nm diameter cobalt powder suspended in glycerol in MALDI-MS for the analysis of protein molecules where the nanoparticles (NPs) are used for desorption and ionization of analytes.[8] Sunner et al. demonstrated the use of graphite microparticles of size 2−200 μm mixed with glycerol as the matrix for the analysis of proteins and peptides, and the procedure is known as a surface-assisted laser desorption/ionization mass spectrometry (SALDI-MS).[9] Later, Wei et al. introduced a matrix free method known as a desorption/ionization on silicon (DIOS) produced by electrochemical etching of silicon surface to ionize the small molecules with no or little chemical background mass signal in the mass spectra.[10] The use of TiO_2 NPs in MALDI-MS

Received: March 10, 2011
Accepted: August 19, 2011
Published: September 06, 2011

has also been reported for desorption and ionization of biomolecules. Lee et al. applied TiO_2 NPs as a matrix for the determination of enediol compounds in tea.[11] Watanabe et al. investigated the photocatalytic cleaning on SALDI-MS with amorphous TiO_2 NPs for the reduction of the background noise and the improvement of the sensitivity of peptides.[12] In addition, gold (Au) NPs are reported for the analysis of a low molecular weight molecule (i.e., glutathione) in SALDI-MS.[13] However, the use of AuNPs as a matrix in SALDI-MS for analysis of small molecules (in the range of 80−500 Da.) showed NP-oriented peaks in the mass spectrum which might affect the sensitivity for the detection of molecules in MS.[14]

As a result of recent advances in nanomaterial preparation, nanomaterial surfaces are used in MALDI imaging mass spectrometry (IMS) for identification and localization of biomolecules in different types of tissue sections. Siuzdak's group has introduced a matrix-free desorption/ionization platform for imaging of biomolecules in tissue samples and named "nanostructure-initiator mass spectrometry (NIMS)".[15] There are other approaches, such as graphite-assisted laser desorption/ionization (GALDI)[16] and DIOS reported for the identification of organic compounds from the tissue surface. Recently, Nanoassisted laser desorption/ionization (NALDI) target plate was introduced for imaging and identification of lipids in mouse brain with very low chemical background.[17] In this scenario, our group has developed a method called nanoparticle-assisted laser desorption/ionization imaging mass spectrometry (Nano-PALDI-IMS) for cellular resolution of cerebellum tissue section to visualize peptides, phospholipids, and metabolites.[18] More recently, silver[19] and gold[20] NPs are used in Nano-PALDI-IMS to identify different types of fatty acids and glycosphingolipids, respectively, in mouse tissue samples which are hardly identified using 2,5-dihydroxybenzoic acid (DHB) as a matrix. However, the simultaneous imaging and detection of LMWM (<500 Da) other than lipid and peptide molecules in biomaterial is still a great challenge at this cutting edge of chemistry and biology.

In the present work, TiO_2 NPs are used as a nanomaterial surface to absorb laser light for effective desorption and ionization of biomolecules in mouse brain using Nano-PALDI-IMS without observing any NP related peaks. TiO_2 NPs are active photocatalytic NPs and have been widely applied in analytical, biochemical, and nanoscience fields.[21] TiO_2 NPs exhibit strong absorption characteristics in the UV region which can be used as a matrix for desorption and ionization of biomolecules.[21,22] The identification of LMWM in tissue sample using TiO_2 NPs is compared with use of DHB and gold NPs as matrixes. MS/MS and capillary electrophoresis mass spectrometry (CE-MS) measurements[23] were also performed on the tissue samples to confirm some of the metabolites found in the brain. The localization patterns of 24 LMWM in mouse brain were demonstrated. The usefulness of the method was also implemented to show the calibration curve for model compound, histidine on the surface of tissue section.

EXPERIMENTAL SECTION

Chemicals. Trifluoroacetic acid (TFA) and titanium(IV) *n*-butoxide were obtained from Sigma (St. Louis, MO). DHB was purchased from Bruker Daltonics (Bremen, Germany). Diammonium hydrogen citrate was obtained from Nacalai Tesque Inc. (Kyoto, Japan). Citric acid and methanol were obtained from Wako Pure Chemicals (Osaka, Japan).

Synthesis of TiO_2 and AuNPs NPs. TiO_2 NPs were prepared as the previously described hydrolysis of titanium(IV) *n*-butoxide in water and ethanol in acidic condition.[21] Briefly, 17 mL of titanium(IV) *n*-butoxide and 8 mL of ethanol were mixed by stirring for 10 min at room temperature. Then, a solution containing 8 mL of ethanol and 375 μL of nitric acid was added dropwise to stirred titanium(IV) *n*-butoxide and solution which was cooled in an ice/water bath under stirring. The concentration of obtained solution of TiO_2 NPs was found to be 1.48 M (Supporting Information). The lower concentrations of NPs (2.42−12.13 mM) were prepared for analysis of mouse brain tissue sections for Nano-PALDI-IMS experiments. The size of the TiO_2 NPs was confirmed using a transmission electron microscope, TEM (JEM 1010), at an accelerating voltage of 80 kV. The TEM image TiO_2 NPs are shown in Supporting Information, Figure S1. AuNPs were synthesized according to ref 14 (Supporting Information).

Solution Preparations. A 97−485 mM DHB solution was prepared by dissolving an appropriate amount of DHB in 1 mL of 75% methanol (containing 0.1% TFA) for MALDI-IMS analysis. Different concentrations of TiO_2 NPs in the range of 2.42−12.13 mM were prepared in 1 mL of methanol from 1.48 M TiO_2 NPs with addition of citrate buffer, 60 μL of diammonium hydrogen citrate (50 mM), and 20 μL of citric acid (100 mM) for Nano-PALDI-IMS analysis. The citrate buffer was added into the TiO_2 NPs to assist the protonation of molecules in MS. Safety steps were maintained during the handling of organic solvents and chemicals used in the experiments.

Preparation of Mouse Brain Tissue Sections. Experimental procedures for mouse samples were performed in accordance with the Animal Experiment Regulations of Hamamatsu University School of Medicine approved by the Science Council of Japan. A male mouse was obtained from Japan SLC (Shizuoka, Japan) and was anesthetized prior to being decapitated. Brain was dissected and frozen in liquid nitrogen and then stored at −80 °C until sectioning of sample. The 15 μm-thick mouse brain tissues were sliced using a cryostat (CM 1950; Leica Microsystems, Wetzler, Germany) at −20 °C, and sections were thaw mounted on indium-tin-oxide (ITO)-coated glass slides. One milliliter of prepared solution of TiO_2 NPs and DHB matrix solution was sprayed on the surface of brain tissue sections using a 0.2 mm nozzle caliber airbrush (Procon Boy FWA Platinum, Tokyo) for MALDI imaging of metabolites.

IMS, MS/MS, and CE-MS Analyses. Imaging of LMWM in mouse brain was performed by an ultraflex II TOF/TOF (Bruker Daltonics) equipped with a 355 nm Nd:YAG laser with a 200 Hz repetition rate. The laser energy used in Nano-PALDI- and MALDI-IMS analyses was 100 μJ. The parameters, such as laser energy, detector gain, and random walk function were first optimized to obtain good sensitivity of the target molecules from the samples. flexImaging software (Version 3.0 obtained from Bruker Daltonics) was used to reconstruct ion images of metabolites at m/z from a whole tissue average spectrum. The mass peaks (at m/z) obtained were normalized to total ion current, and then, peak intensity was taken in account to study the distribution of molecules in tissue section. Before performing the MALDI imaging experiment in TOF/TOF-MS, the instrument was calibrated with DHB, bradykinin, and angiotensin II at m/z 155.03 $[M+H]^+$, 757.39 $[M+H]^+$, and 1046.54 $[M+H]^+$ in the positive ion mode. The mixture of DHB, bradykinin, and angiotensin II was deposited near to the brain tissue section for calibration of the instrument in order to avoid the mass error

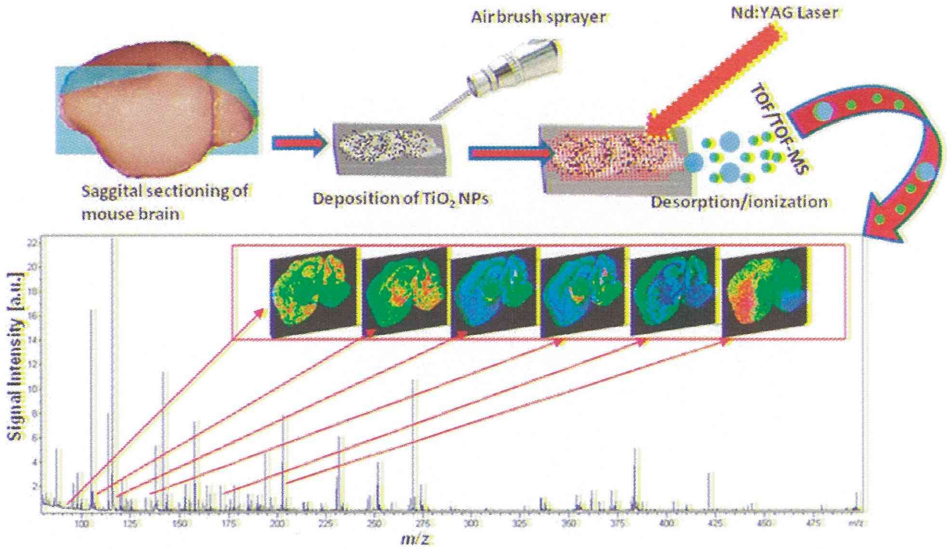

Figure 1. Work flow of Nano-PALDI-IMS experiment. The 15 μm-thick mouse brain tissues were sliced using a cryostat and thaw mounted on ITO coated glass slides, and the TiO_2 NPs were applied on the surface of tissue section and followed by Nano-PALDI-IMS analyses.

for extended and uneven tissue section prior to imaging. We also confirmed the MS/MS analyses of LMWM in mouse brain tissue section using Q-TOF-MS. Capillary electrophoresis (CE)-MS based analyses were performed for confirmation of LMWM using Agilent CE systems equipped with a time-of-flight mass spectrometer (TOF-MS) and a built-in diode-array detector (Agilent Technologies). The details of sample preparation, capillary type, and instrumental conditions can be found in the Supporting Information.[23]

Sample-to-Sample Reproducibility in Mouse Tissue. Sample-to-sample reproducibility for Nano-PALDI-IMS and MALDI-IMS analyses of LMWM were calculated in terms of relative standard deviation percentage (±RSD,%) which presented the precision of the proposed method. For this, 0.2 μg/mm^3 of histidine was deposited on the three serial section of brain tissue (n = 3), and imaging experiments were performed using TiO_2 NPs and DHB as a matrix. The region of interest (ROI) was selected from triplicate analyses, and mean intensity was used to calculate the RSD, %. The calculation for RSD % of TiO_2 NPs and DHB is given in the Supporting Information.

Quantitative Analysis of Histidine in Mouse Tissue. To establish a calibration curve, different concentrations of histidine (0.1, 0.2, 0.4, 0.8, and 1.6 μg/mm^3) were spotted on the surface of brain tissue section and TiO_2 NPs were deposited using an airbrush followed by Nano-PALDI-IMS. The number of analyses of tissue sections was performed three times (n = 3) at each concentration. The region of interest (ROI) selected and average intensity from each concentration of histidine (at m/z 156.08) was exported using a script program (included in the flexAnalysis, Bruker Daltonics). The average intensity (n = 3) of each concentration was used to construct the calibration curve for histidine in tissue section.

RESULTS AND DISCUSSION

In the present work, Nano-PALDI-IMS was applied for simultaneous imaging of LMWM (<500 Da) in brain tissue after applying TiO_2 NPs on the surface of tissue section for effective desorption and ionization of molecules. TiO_2 NPs has been widely used as a transition-metal oxide, which is characterized by a filled valence band and an empty conduction band. Thus, the laser energy absorbed by TiO_2 NPs is most likely converted to thermal energy through the formation of charge carrier and then transferred to the top layer of the tissue surface for the desorption/ionization process.[22,24] Molecules present on the discrete spots or the pixel are ionized using laser energy in the raster fashion. Figure 1 shows the work flow of the Nano-PALDI-IMS imaging experiment.

Analysis of Mouse Brain. Mouse brain was selected for imaging of LMWM in tissue section using TiO_2 NPs as a matrix for desorption/ionization of molecules. Figure 2a represents the sagittal section of HE-stained mouse brain showing cerebellar cortex (CBX), corpus striatum (CP), cerebral cortex (CTX), hippocampus formation (HPF), and thalamus (TH). TiO_2 NPs (Figure 2b) and DHB (Figure 2c) were deposited on the surface of brain tissue sections and analyzed at a scan pitch of 70 μm in the positive ion mode followed by the reconstruction of ion images. The regions of mouse brain could be differentiated after the deposition of TiO_2 NPs due to the formation of a very thin layer of coating of NPs on the surface of a tissue section as the size of NPs was <10 nm. Conversely, the structure of mouse brain can be hardly examined after the deposition of DHB matrix due to the thick layer deposition of matrix on the surface of the tissue section (crystal size of the matrix is found to be 50 μm).[25]

The ionization efficiency of analyte molecules greatly depends on the concentration of NPs and DHB matrixes used in SALDI-MS[14] and MALDI-MS, respectively. Thus, the concentrations of TiO_2 NPs and DHB matrix were optimized for efficient desorption/ionization of molecules from the surface of brain tissue (Supporting Information, Figures S2 and S3). The mass spectra of LMWM obtained using TiO_2 NPs and DHB as a matrix are shown in Figure 3a,b, respectively. In Figure 3a, the ion signals were generated at m/z 137.01, 155.03, 177.04, 230.05, 273.02, 352.78, and 382.76 which are corresponding to $[DHB - H_2O + H]^+$, $[DHB + H]^+$, $[DHB + Na]^+$, $[DHB + 2K - H]^+$, $[2DHB - 2H_2O + H]^+$, $[2DHB + 2Na - H]^+$, and $[2DHB + 2K - H]^+$,

dx.doi.org/10.1021/ac201602s |Anal. Chem. 2011, 83, 7283–7289

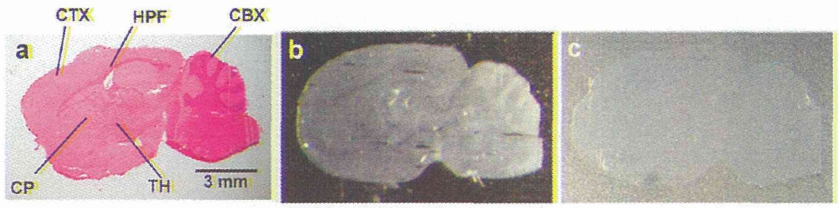

Figure 2. Sagittal section of mouse brain (a): HE-stained mouse brain showing cerebellar cortex (CBX), corpus striatum (CP), cerebral cortex (CTX), hippocampus formation (HPF), and thalamus (TH). (b) Deposited with TiO_2 NPs. (c) Deposited with DHB matrix, with 3 mm scale bar (black color line).

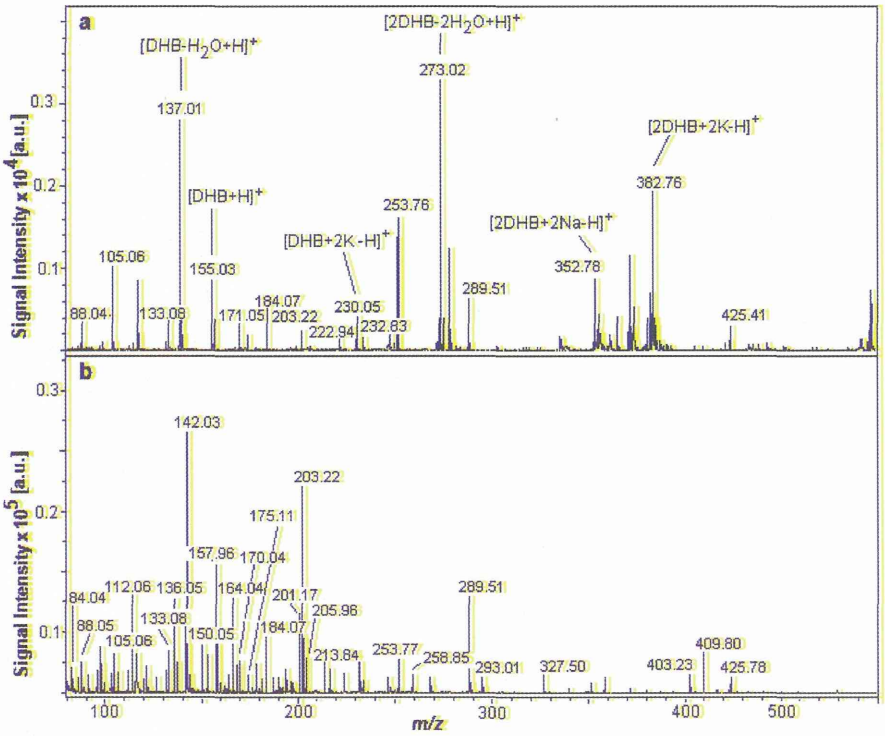

Figure 3. Mass spectra of LMWM in detected in mouse brain tissue section obtained with (a) DHB in MALDI-IMS and (b) TiO_2 NPs in Nano-PALDI-IMS.

respectively. The signals produced from DHB in MALDI-MS might influence both the interpretation of metabolites in mass spectra and the sensitivity for the detection. Less than 25 biomolecule signals were obtained using DHB as a matrix. However, 200 biomolecule signals with higher signal intensity were observed using TiO_2 NPs without any NP related peaks, shown in Figure 3b. The control experiment was also performed by depositing TiO_2 NPs on the ITO glass slide and no any NP-oriented peaks were observed in the mass spectrum (Supporting Information, Figure S4). The mass peaks (m/z) obtained in the mass spectrum were reconstructed to form ion images using flexImaging software. We were able to reconstruct the distribution of metabolites in mouse brain where 179 molecule signals were specific to TiO_2 NPs (Figure 4a and Supporting Information, Figure S5a–c); 4 were specific to DHB (Supporting Information, Figure S6); and 21 were common to both TiO_2 NPs and DHB matrix (Figure 4b and Supporting Information, Figure S7). We also analyzed a standard compound such as serine, cysteine, and tyrosine to check the fragmentation of any detected molecules in brain tissue section using TiO_2 NPs at the same laser energy (100 μJ) used for the IMS experiments. For this, 1 μL of serine, cysteine, and tyrosine (50 ng/μL) with the same amount of NPs were deposited on the target plate followed by the MS analysis. The results showed no fragmentation of molecules in the mass spectrum when TiO_2 NPs was used as a matrix (Supporting Information, Figure S8a–c). This enabled us to conclude that the use of TiO_2 NPs is effective for ionization of biomolecules from the surface of brain tissue.

Localization of LMWM in Mouse Brain. The selected ion images of metabolites in Figure 4 showed the structure of mouse brain with distinguishable localization of ion distribution in different compartments of the brain section. The ion images found for putrescine at m/z 89.10 $[M + H]^+$, γ-aminobutyric acid at m/z 104.06 $[M + H]^+$, uracil at m/z 113.03 $[M + H]^+$, ornithine at m/z 133.08 $[M + H]^+$, and hypoxanthine at m/z 137.05 $[M + H]^+$ were specific to gray matter region of the mouse brain which

dx.doi.org/10.1021/ac201602s |Anal. Chem. 2011, 83, 7283–7289

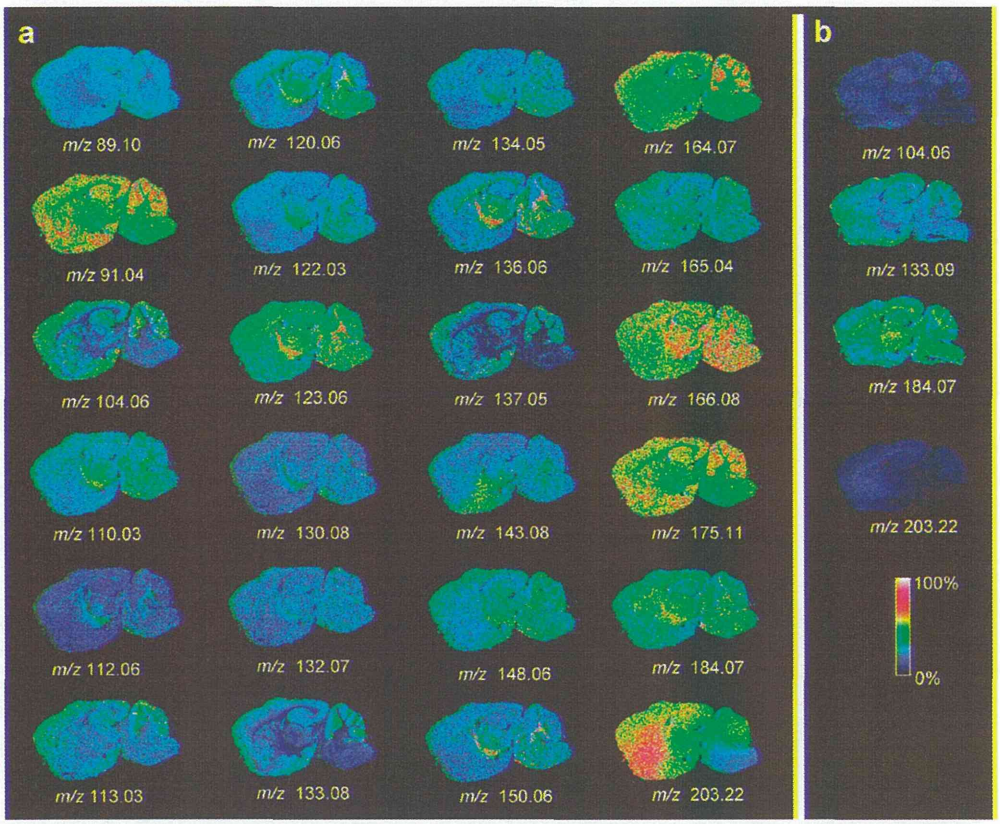

Figure 4. Ion images of LMWM in mouse brain obtained with (a) TiO_2 NPs in Nano-PALDI-MS and (b) DHB matrix in MALDI-MS.

exhibited almost the same type of ion distribution. The white matter of the mouse brain can be differentiated by ion images of cytosine at m/z 112.06 $[M + H]^+$, threonine at m/z 120.06 $[M + H]^+$, pipecolic acid at m/z 130.08 $[M + H]^+$, adenine at m/z 136.06 $[M + H]^+$, and phenylalanine at m/z 166.08. The lobular structure of the cerebellum can be distinguished by ion images of γ-aminobutyric acid at m/z 104.06 $[M + H]^+$, ornithine at m/z 133.08 $[M + H]^+$, hypoxanthine at m/z 137.05 $[M + H]^+$, and *S*-methylmethionine at m/z 164.07. The most intense ion was observed at the striatum region of the mouse brain for spermine at m/z 203.22 $[M + H]^+$, and some white matter specific region was examined for phosphorylcholine at m/z 184.07 $[M]^+$ in thalamus and cerebellum, whereas the creatine acid at m/z 132.07 $[M + H]^+$ showed almost an uniform distribution of ions across the tissue section. This data set indicates the region-specific studies of LMWM and provides important information for performing such analyses in mouse brain.

MS/MS and CE-MS Analysis of LMWM in Mouse Brain. MS/MS analyses of five molecules, such as, γ-aminobutyric acid, phosphorylcholine, cytosine, threonine, and creatine, in positive ion mode are illustrated in the Supporting Information, Figures S9–S13. Other assigned molecules were validated using CE-MS compared with respective standard compounds (Supporting Information, Table S1). The detected molecules in brain tissue sample were matched against known Human Metabolome Database Search maintained Genome Alberta and Genome Canada (http://www.hmdb.ca) and KEGG GenomeNet Database Resources (http://www.genome.jp).

Reproducibility and Quantitative Analysis. Sample-to-sample reproducibility (RSD) obtained for analysis of histidine in tissue section was ±12.1 and ±26.7% using TiO_2 NPs and DHB matrix, respectively. A higher percentage of RSD (±26.7%) showed a large variation of signal height when DHB matrix was used as a matrix probably due to the heterogeneous crystal formation of matrix with sample. However, a lower value of RSD (±12.1%) represented a small variation in signal intensity during the imaging of LMWM using NPs, possibly due to the homogeneous thin crystal formation of NPs on the surface of tissue. This heterogeneous distribution of DHB crystals and uniform distribution of NPs was also reported by Taira et al., in Nano-PALDI-IMS analysis of biomolecules.[18] From these results, we can conclude that a good value of sample reproducibility was obtained when TiO_2 NPs as a matrix was compared to DHB in IMS analyses. Thus, the TiO_2 NPs were demonstrated for quantitative analysis of histidine from the surface of tissue section. The ion images for different concentrations of histidine obtained from the brain tissue section are shown in Figure 5a. The linear range for histidine was found between 0.1 and 1.6 $\mu g/mm^3$ with the correlation of estimation <0.998, shown in Figure 5b. This suggests that the quantitative analysis can be performed using a Nano-PALDI-IMS for the determination of LMWM in brain tissue sample.

Comparison for Imaging of LMWM in Mouse Brain Using TiO_2 NPs, DHB, and AuNPs as a Matrix. We compared the identification of LMWM using TiO_2 NPs in Nano-PALDI-IMS with MALDI-IMS using DHB matrix. Figure 4a,b and Figure S7 (Supporting Information) show the ion images of LMWM in the mouse brain tissue section using TiO_2 NPs and DHB as a matrix. A number of LMWM with good signal intensity were obtained

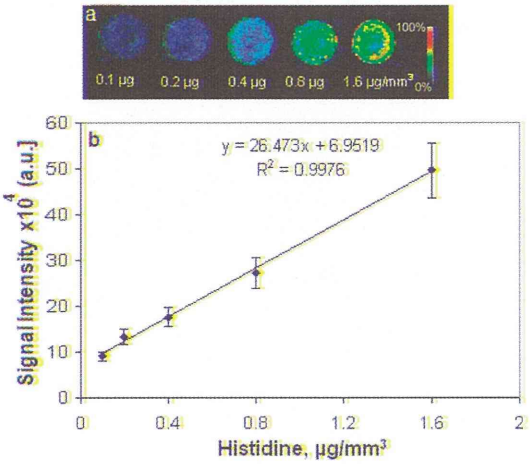

Figure 5. Ion images of histidine (at 0.1, 0.2, 0.4, 0.8, and 1.6 $\mu g/mm^3$) obtained from the brain tissue section using Nano-PALDI-IMS (a). The linear range for histidine was found between 0.1 and 1.6 $\mu g/\mu m^3$ with the correlation of estimation <0.9977 (b). The error bar represented as the mean ± standard deviation (n = 3).

when TiO_2 NPs was used as a matrix in Nano-PALDI-IMS as compared to the use of DHB in MALDI-IMS analysis. The reason for obtaining a higher signal intensity and number of metabolites using TiO_2 NPs is due to the thin coating of NPs on the surface of the brain tissue section that may have caused an efficient absorption and transfer of the light energy for desorption and ionization of molecules from the surface of tissue section. Taira et al. also reported the detection of a higher number of biomolecules from the surface of tissue sample when a small size of NPs was used as a matrix in Nano-PALDI-IMS.[18] The biomolecules at m/z 104.06, 133.08, 184.07, and 203.22 (shown in Figure 4) were detected by both approaches where the distribution of ion pattern were found to be same, though the signal intensity of ion images formed using DHB was less intense than that using the TiO_2 NPs. These results confirmed the ability of TiO_2 NPs in detecting a number of molecule signals in brain tissue when used in Nano-PALDI-IMS.

In addition, we also performed an imaging of mouse brain without use of TiO_2 NPs in laser desorption ionization (LDI-MS) and AuNPs in SALDI-MS to detect a LMWM from the tissue section at the same laser energy used in the Nano-PALDI-IMS experiments. LDI-MS is reported to be a matrix free technique for analysis of low molecular biomolecules from tissue surface. However, when LDI-IMS (without use of TiO_2 NPs as a matrix) was applied for analysis of biomolecules, no signal was detected from the surface of mouse brain tissue. Next, we applied AuNPs on the surface of brain tissue section and IMS analysis was performed at the optimal conditions. Figure S14 (Supporting Information) shows the mass spectrum of LMWM in tissue section using AuNPs for desorption/ionization in SALDI-IMS. The AuNP-oriented peaks at m/z 196.96 (Au^+) and 393.92 (Au_2^+) were observed in the mass spectrum (80−500 Da) using AuNPs as a matrix which might have caused the suppression of LMWM signals in the mass spectrum. However, higher number molecular signals were obtained without any NP-related peaks using TiO_2 NPs for analysis of mouse brain tissue.

Comparison of Nano-PALDI-IMS with other Imaging Studies. Finally, we illustrated the progress of imaging methods for analysis of biomolecules in tissue samples as compared to Nano-PALDI-IMS analysis. Northen et al. exploited the clathrate nanostructure surface for the identification and imaging of various types of small molecules in mass spectrometry for sensitive detection of molecules from the sample in NIMS.[15] However, the procedure used for sample preparation was found to be tedious, requiring multisteps and was expensive as compared to Nano-PALDI-IMS analysis. Recently, Benabdellah et al. developed a method called "chemical mass spectrometry imaging" to determine the localization of 13 primary metabolites in rat brain using MALDI-IMS, in addition to a few matrix oriented peaks in the mass spectrum.[26] More recently, Shrestha et al. reported the direct analysis of LMWM in mouse brain using atmospheric pressure-infrared matrix-assisted laser desorption ionization (AP-IR-MALDI) and laser ablation electrospray ionization-mass spectrometry (LAESI-MS) for the detection of 40 metabolites with lack of imaging data.[27] In addition, Nemes et al. demonstrated the simultaneous imaging of 200 small metabolites and lipids in rat brain using LAESI-MS where half of the molecules were found to be lipid molecules.[28] The use of secondary ion mass spectrometry (SIMS) for imaging of low molecular weight biomolecules in tissue samples was established for higher spatial resolution (a few 100 nm).[29] The fragmentation of polar headgroup was reported in SIMS as well as the inability to perform MS/MS analyses to confirm the molecules.[30] We also compared our results with the sublimation method for depositing matrix on the surface of brain tissue for imaging of phospholipids in mouse brain where the number of detected signals were found to be less compared to the signals obtained by the proposed method.[31] Shroff et al. investigated the use of 1,8-bis(dimethyl-amino) naphthalene (DMAN; proton sponge), as a novel matrix for MALDI-MS analysis of anions in negative ion mode. The potential of ionless matrixes was target for profiling plant leaf with a 108 monoisotpic peaks in the mass spectrum.[32] On the other hand, in this investigation, TiO_2 NPs were synthesized in a simple and single step approach and were directly used for imaging studies for simultaneously imaging of LMWM (<500 Da).

CONCLUSIONS

We believe that the use of TiO_2 NPs in Nano-PALDI-IMS exhibits advantages of simple sample preparation, matrix free background, and detection of a higher number of LMWM signals from the tissue sample. The potentiality of TiO_2 NPs is compared with DHB and gold NPs for imaging of LMWM in tissue samples, and the use of TiO_2 NPs is found to be better in sensitivity and detecting a higher number of biomolecule signals as compared to conventional DHB and gold NPs as matrixes. Finally, the present approach is also demonstrated as a simple, rapid, and inexpensive method for imaging of LMWM in tissue sample as compared to other existing methods such as LDI-MS, NIMS, and LAESI-MS. Nano-PALDI-IMS using TiO_2 NPs can be a useful tool in elucidating the novel findings pertaining to biomarkers of the diseases in biological tissue samples.

ASSOCIATED CONTENT

Supporting Information. Additional information as noted in text. This material is available free of charge via the Internet at http://pubs.acs.org.

AUTHOR INFORMATION

Corresponding Author
*Tel/Fax: +81-53-435-2292. E-mail: setou@hama-med.ac.jp.

ACKNOWLEDGMENT

We would like to thank the Japanese society for the Promotion of Science, Japan, for a postdoctoral fellowship (to K.S.). This work was also supported by a Grant-in-Aid for SENTAN from the Japan Science and Technology Agency (to M.S.). CE-MS analysis was supported by a grant for leading metabolome research 2010 provided by Human Metabolomics Technology (http://humanmetabolome.com/) to Y.S.

REFERENCES

(1) Sugiura, Y.; Konishi, Y.; Zaima, N.; Kajihara, S.; Nakanishi, H.; Taguchi, R.; Setou, M. *J. Lipid Res.* **2009**, *50*, 1776–1788.
(2) Weissleder, R.; Pittet, M. J. *Nature* **2008**, *452*, 580–589.
(3) Blow, N. *Nat. Methods* **2008**, *5*, 981–987.
(4) Jansen, J. F.; Backes, W. H.; Nicolay, K.; Kooi, M. E. *Radiology* **2006**, *240*, 318–332.
(5) Bourcier, S.; Benoist, J. F.; Clerc, F.; Rigal, O.; Taghi, M.; Hoppilliard, Y. *Rapid Commun. Mass Spectrom.* **2006**, *20*, 1405–1421.
(6) Petyuk, V. A.; Qian, W. J.; Smith, R. D.; Smith, D. J. *Methods* **2010**, *50*, 77–84.
(7) Karas, M.; Hillenkamp, F. *Anal. Chem.* **1988**, *60*, 2299–2301.
(8) Tanaka, M.; Waki, H.; Ido, Y.; Akita, S.; Yoshida, T. *Rapid Commun. Mass Spectrom.* **1988**, *2*, 151–153.
(9) Sunner, J.; Dratz, E.; Chen, Y. C. *Anal. Chem.* **1995**, *67*, 4335–4342.
(10) Wei, J.; Buriak, J. M.; Siuzdak, G. *Nature* **1993**, *399*, 243–246.
(11) Lee, K. H.; Chiang, C. K.; Lin, Z. H.; Chang, H. T. *Rapid Commun. Mass Spectrom.* **2007**, *21*, 2023–2030.
(12) Watanabe, T.; Okumura, K.; Kawasaki, H.; Arakawa, R. *J. Mass. Spectrom.* **2009**, *44*, 1443–1451.
(13) Chiang, C. K.; Chiang, N. C.; Lin, Z. H.; Lan, G. Y.; Lin, Y. W.; Chang, H. T. *J. Am. Soc. Mass Spectrom.* **2010**, *21*, 1204–1207.
(14) Su, C. L.; Tseng, W. L. *Anal. Chem.* **2007**, *79*, 1626–1633.
(15) Northen, T. R.; Yanes, O.; Northen, M. T.; Marrinucci, D.; Uritboonthai, W.; Apon, J.; Golledge, S. L.; Nordstrom, A.; Siuzdak, G. *Nature* **2007**, *449*, 1033–1036.
(16) Cha, S.; Yeung, E. S. *Anal. Chem.* **2007**, *79*, 2373–2385.
(17) Vidova, V.; Novak, P.; Strohalm, M.; Pol, J.; Havlicek, V.; Volny, M. *Anal. Chem.* **2010**, *82*, 4994–4997.
(18) Taira, S.; Sugiura, Y.; Moritake, S.; Shimma, S.; Ichiyanagi, Y.; Setou, M. *Anal. Chem.* **2008**, *80*, 4761–4766.
(19) Hayasaka, T.; Goto-Inoue, N.; Zaima, N.; Shrivas, K.; Kashiwagi, Y.; Yamamoto, M.; Nakamoto, M.; Setou, M. *J. Am. Soc. Mass Spectrom.* **2010**, *21*, 1446–1454.
(20) Goto-Inoue, N.; Hayasaka, T.; Zaima, N.; Kashiwagi, Y.; Yamamoto, M.; Nakamoto, M.; Setou, M. *J. Am. Soc. Mass Spectrom.* **2010**, *21*, 1940–1943.
(21) Chen, X.; Mao, S. S. *Chem. Rev.* **2007**, *107*, 2891–2959.
(22) Gholipour, Y.; Giudicessi, S. L.; Nonami, H.; Erra-Balsells, R. *Anal. Chem.* **2010**, 82, 5518–5526.
(23) Sugiura, Y.; Taguchi, R.; Setou, M. *PLoS One* **2011**, *6*, e117952.
(24) Lorkiewicz, P.; Yappert, M. C. *Anal. Chem.* **2009**, *81*, 6596–6603.
(25) Garden, R. W.; Sweedler, J. V. *Anal. Chem.* **2000**, *72*, 30–36.
(26) Benabdellah, F.; Touboul, D.; Brunelle, A.; Laprevote, O. *Anal. Chem.* **2009**, *81*, 5557–5560.
(27) Shrestha, B.; Nemes, P.; Nazarian, J.; Hathout, Y.; Hoffman, E. P.; Vertes, A. *Analyst* **2010**, *135*, 751–875.
(28) Nemes, P.; Woods, A. S.; Vertes, A. *Anal. Chem.* **2010**, *82*, 982–988.
(29) Altelaar, A. F.; Klinkert, I.; Jalink, K.; de Lange, R. P.; Adan, R. A.; Heeren, R. M.; Piersma, S. R. *Anal. Chem.* **2006**, *78*, 734–742.
(30) Yang, H. J.; Sugiura, Y.; Ishizaki, I.; Sanada, N.; Ikegami, K.; Zaima, N.; Shrivas, K.; Setou, M. *Surf. Interface Anal.* **2010**, *42*, 1606–1611.
(31) Hankin, J. A.; Barkley, R. M.; Murphy, R. C. *J. Am. Soc. Mass Spectrom.* **2007**, *18*, 1646–1652.
(32) Shroff, R.; Rulísek, L.; Doubsky, J.; Svatos, A. *Proc. Natl. Acad. Sci.* **2009**, *106*, 10092–10096.

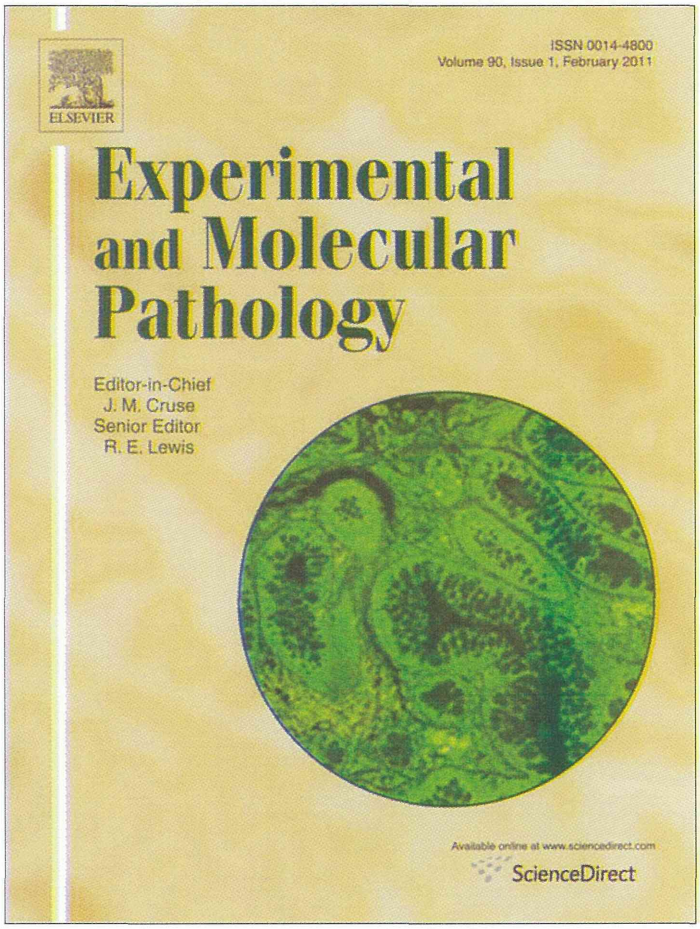

(This is a sample cover image for this issue. The actual cover is not yet available at this time.)